Jordi Piella, Neus G. Bastús* and Víctor Puntes*

Modeling the Optical Responses of Noble Metal Nanoparticles Subjected to Physicochemical Transformations in Physiological Environments: Aggregation, Dissolution and Oxidation

DOI 10.1515/zpch-2016-0874
Received August 10, 2016; accepted October 11, 2016

Abstract: Herein, we study how optical properties of colloidal dispersions of noble metal nanoparticles (Au and Ag) are affected by processes such as aggregation and oxidative dissolution. The optical contributions of these processes to the extinction spectra in the UV-vis region are often overlapped, making difficult its interpretation. In this regard, modeling the UV-vis spectra (in particular absorbance curve, peaks position, intensity and full width at half maximum -FWHM) of each process separately offers a powerful tool to identify the transformation of NPs under relevant and complex scenarios, such as in biological media. The proper identification of these transformations is crucial to understand the biological effects of the NPs.

Keywords: nanoparticles; optical properties; physicochemical transformations.

1 Introduction

Noble metal nanoparticles (NPs), particularly Au and Ag NPs, are the most widely used nanomaterials, having recognized importance in chemistry, physics, and

***Corresponding authors: Neus G. Bastús,** Institut Català de Nanociència i Nanotecnologia (ICN2), CSIC and The Barcelona Institute of Science and Technology (BIST), Campus UAB, 08193, Bellaterra, Barcelona, Spain, e-mail: neus.bastus@icn2.cat; and **Víctor Puntes,** Institut Català de Nanociència i Nanotecnologia (ICN2), CSIC and The Barcelona Institute of Science and Technology (BIST), Campus UAB, 08193, Bellaterra, Barcelona, Spain; Vall d'Hebron Institut de Recerca (VHIR), 08035, Barcelona, Spain; and Institut Català de Recerca i Estudis Avançats (ICREA), 08010 Barcelona, Spain, e-mail: victor.puntes@icn2.cat
Jordi Piella: Institut Català de Nanociència i Nanotecnologia (ICN2), CSIC and The Barcelona Institute of Science and Technology (BIST), Campus UAB, 08193, Bellaterra, Barcelona, Spain; and Universitat Autònoma de Barcelona, Campus UAB, 08193 Bellaterra, Barcelona, Spain

biology because of their outstanding optical, electrical, and photothermal properties. These unique properties, together with the high reactivity of the NPs and their affinity for binding many (bio)molecules makes them attractive candidates for a wide variety of uses, (bio)applications and array of commercial products, including sensing, diagnostic, labeling and antimicrobial agents [1–3].

A key challenge on the applicability of the NPs relies on the ability to integrate these NPs in biological systems. A significant number of biological systems are complex aqueous media composed of electrolytes, proteins and metabolites, which are able to interact with the inorganic surface of the NPs promoting different physicochemical transformations that modify their biological responses and may ultimately lead to unexpected (including adverse and toxic) effects [4, 5]. Indeed, there have been growing concerns regarding the release of nanomaterials to the environment [6] and the potential adverse health effects of exposure to NPs [6–9]. These transformations also represent a post-synthetic tool to rationally design the final fate of the NPs. Thus, depending on the final applicability, NPs are preferred to be persistent (ex. implants) or degradable (ex. antibacterial), and the extent of this persistency along with the elimination and accumulation of the NPs in the different organs, ultimately depends on the time-dependent physicochemical changes of the morphology of NPs, their surface chemistry and aggregation state. Therefore, a significant challenge when designing NPs for a desired purpose and evaluating their health implications is the study of the complex set of physical and chemical transformations that NPs inevitably undergo, driven by their high reactivity, when they are exposed to different environments.

Due to their higher percentage of surface atoms and their colloidal nature, NPs experience processes that transform them towards more stable thermodynamic states at a faster time scale than their bulk counterparts [10, 11], which is translated into high rates of aggregation, oxidation, dissolution and interaction with proteins [4, 8, 10, 12–14]. Aggregation, that is colloidal stability, has a significant influence on the reactivity, bioavailability and pharmacokinetic of NPs, having long been recognized to mediate the toxicity of the particles, as in the case of asbestiform materials, industrial aerosols, and ambient particulate matter [15]. Similarly, oxidative dissolution [16] favors the chemical dissolution of NPs, affecting their persistence and promoting the release of ionic species [12, 17, 18], which in the case of Ag NPs includes metallic silver (Ag^0), ionic silver (Ag^+), and silver chloride (AgCl)) and are responsible for their bactericidal effect [7, 9, 19–22]. The physicochemical state of NPs also plays a role in their interaction with media proteins, and the subsequent nature of the protein corona around the NPs [23, 24] (the so-called *soft* and *hard* corona), inevitably providing them with new biological identity [25, 26], which determines their physiological response including

cellular uptake, biodistribution and toxicity [27, 28]. The extent of each individual process is determined by the intrinsic properties of the NPs (material, size, shape, concentration, crystallinity, surface charge and coating) and the nature (ionic strength, pH) in which they are dispersed. While these processes can be studied separately [4], the greatest NP transformations occur within the same time scale [29] (from minutes to hours of exposure) and translated into the overlapping and competition between all the different processes involved. Thus, it is common to observe that NPs are instable and tend to aggregate after their exposition to cell culture media and that they corrode while being coated by proteins. As a result of this complexity, it is critical to fully understand the transformation of NPs after exposition, not only to better interpret the biological effect of the NPs but also to better able to design NPs for a specific purpose.

Optical properties, in particular UV-vis spectra and localized surface plasmon resonances (LSPRs), are easily measurable signatures of metal NPs indicative of their morphology (size and shape), composition, surface chemistry and aggregation state that can be used to identify chemical transformation processes [30–35]. Since they are wide applied in plasmonic technologies, including therapy, detection and sensing [31, 36–38], it is important to understand how these optical signatures are affected by processes such as aggregation, dissolution, oxidation and protein adsorption. In this regard, the analysis of the UV-vis spectra (in particular absorbance curve, LSPR peak positions, intensity and full width at half maximum -FWHM), is a powerful tool to characterize the evolution of the NPs in biological media.

In this context, we herein model and study the time-dependent optical properties, in particular the UV-vis spectra, of Au and Ag NPs after different physicochemical transformation processes, focusing on the evolution of the LSPR peaks upon aggregation, oxidative dissolution and protein adsorption. Calculations are based on the standard Mie theory of spherical particles using MiePlot software and MultiLayer NP Simulator platform freely available online [39]. The most characteristics features of each process are described and discussed, in particular for aggregation and oxidative dissolution, in order to separately analyze the different optical responses. Obtained results can be used as a qualitative guide to identify the evolution of Au and Ag NPs in biological environments.

2 Materials and methods

Calculations: Calculations of the extinction efficiency (Q_{ext}) of Ag and Au NPs of different diameters in water at 25 °C were obtained using MiePlot software and

MultiLayer NP Simulator platform freely available online [39, 40]. The dielectric constant and refractive index of the metal were that provided by the programs while for the oxides the data were extracted from the literatures [41]. The Q_{ext} was correlated with the empirical value of extinction, or absorbance, (A) through the Beer-Lambert law using the following equation:

$$A = \varepsilon c l \tag{1}$$

where ε is the extinction coefficient of the solution in units (M^{-1} cm^{-1}), c is the molar metal atom concentration and l (cm) is the path length of the beam of light through the solution. For particles of radi r (cm), the extinction coefficient can be expressed by:

$$\varepsilon = \frac{3V_m Q_{ext}}{4\ln(10)r} \tag{2}$$

Where V_m (M^{-1}) is the molar volume of the metal and Q_{ext} is the above defined dimensionless extinction efficiency.

$$Q_{ext} = \frac{\text{extinction cross section}}{\text{cross sectrion}} = \frac{\sigma_{ext}}{\pi r^2} \tag{3}$$

For colloidal solutions of NPs composed by particles of different sizes, as well as, to account for the polydispersity, the calculated absorption spectra was that resulting from the sum of the spectrum for each NP diameter multiplied by the mass fraction they represent in the solution.

3 Results and discussion

3.1 Optical properties of noble metal nanoparticles

The ability of NPs to interact resonantly with light is usually expressed in terms of extinction efficiency (Q_{ext}), which is the sum of two mechanisms -absorption and scattering- and stands for the loss of light from a transmitted beam. The Q_{ext} is a theoretically and dimensionless parameter strongly dependent on the particle size and chemical composition which is usually plot in LSPRs calculations. Moreover, when working with colloidal dispersions of NPs the empirical value of extinction, also called absorbance when referred to experimental results, is commonly used. Both terms are empirically related through the Lambert-Beer law. For small NPs and molecular species there is no appreciable scattering contribution

and therefore the experimentally measured extinction coincides with the absorption term (see calculation section). Beyond the information from Q_{ext}, extinction term contents quantitative information about particle concentration (a solution diluted twice has the same Q_{ext} but not the same extinction), which results in an additional and interesting parameter when assessing possible transformation of the NPs. In order to facilitate comparison between the calculations herein presented and the available experimental results, all calculated spectra is plotted through the extinction, something usually omitted in many published works.

When comparing the calculated extinction spectra for NPs of different sizes one has to consider if the results are plotted with the total mass concentration of the particles kept constant or in relation to the total number concentration of the particles in solution. Depending on the process of study (aggregation, coalescence, dissolution, oxidation or protein adsorption) one selection is preferred to the other. Thus, the evolution of the extinction spectra in processes such as aggregation or coalescence is better explained considering the total mass of the NPs kept constant while the number of NPs in solution constantly changes since they coalesce forming large clusters. Conversely, for other processes such as oxidation and dissolution, the number of particles is constant at the initial stages but not their total mass. All of these considerations affect not only the Q_{ext}, which is dependent on the chemical composition and size distribution of the NPs, but also the absolute extinction intensity, which depends on the total mass and the total number of the particles, arising as an interesting additional signature of these processes.

3.2 Calculated absorbance spectra of a monodisperse colloidal solution of metal nanoparticles considering constant particle mass concentration

Figure 1 shows the calculated size-dependent spectra of colloidal solutions of monodisperse Ag and Au NPs with sizes between 10 and 200 nm considering a constant particle mass concentration. In these conditions, the concentration number of NPs decreases as increasing the NP size, being higher for small particles and lower for larger ones. As can be seen, the dipolar LSPR band is clearly visible. Its position depends on NP size and composition, peaking between 380 and 800 nm for Ag NPs, and between 500 nm and 800 nm for the Au NPs (Figure 1a, b). Besides, the peak broadens and red-shifts as NP size increases for both metals (Figure 1c), which can be explained according to the Mie theory [42–44].

Beyond this broadening and red-shift of the LSPR, the extinction intensity modulates its value after modifications of NP size. Thus, the extinction of Ag NPs

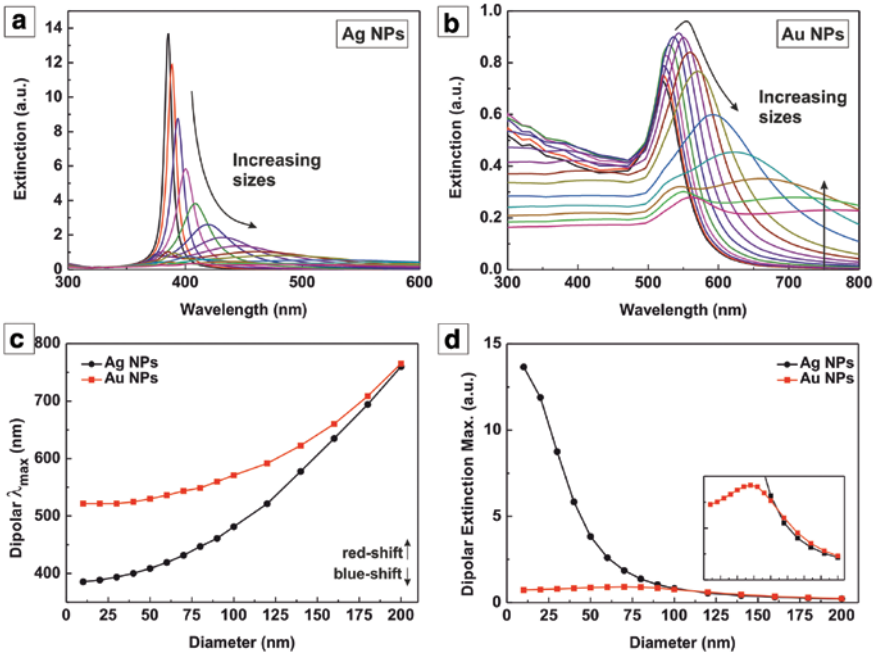

Fig. 1: Calculated extinction spectra of Ag (a) and Au (b) NPs of different sizes from 10 nm to 200 nm at equal total particle mass concentration. The concentration of metal atoms is 0.16 mM and the light pathway 1 cm. Dipolar LSPR peak position (c) and extinction maximum (d) as a function of NP diameter for Ag and Au NPs. In both cases a red-shift is observed in the LSPR as increasing NP size. On the other hand, the maximum extinction drastically drops for increasing Ag sizes while it is almost constant for Au NPs. For larger sizes, both curves evolve similarly which is indicative that scattering becomes relevant and dominates the overall shape of the curve. The differences between both metals are due to the different ability of NP to absorb light, stronger in Ag than Au NPs.

is maximized for particles of 10 nm, and then drastically drops for increasing sizes (Figure 1d). This is translated into the fact that it is easier to detect the presence of Ag NPs by UV-vis spectra when they are in the form of many small particles rather than distributed in a few larger ones. Interestingly, this maximum absorbance value is shifted to particles of 70 nm in the case of gold, being much less pronounced and remaining rather constant. Remarkably, for larger sizes, both curves evolve similarly, which is indicative of dominance of the scattering processes.

An important consequence derived from these results is the different sensitivity of the UV-vis spectra to "detect" and monitor particles of large sizes in a mixed colloidal solution. In this regard, a fraction of larger particles results in higher modifications in the absorbance curve in the case of Au than Ag.

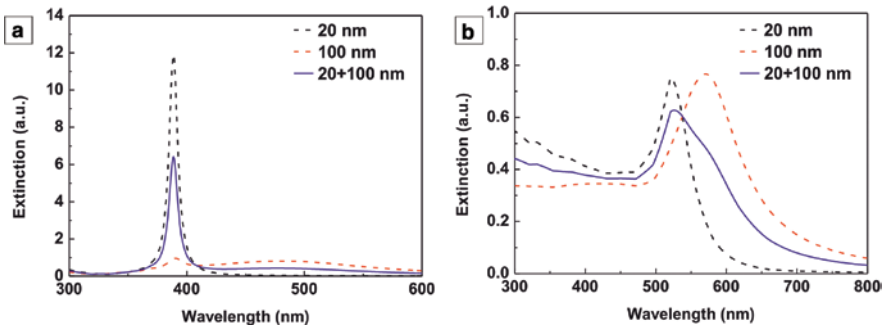

Fig. 2: Calculated extinction spectra of "mixed" solutions of NPs with different size for Ag (a) and Au (b) NPs. Spectra were calculated considering equal mass concentration of the particles. The concentration of metal atoms is 0.16 mM and there is 50% in mass of each size (20 nm and 100 nm). The light pathway is 1 cm.

Figure 2 exemplifies this point by plotting the extinction of a mixed colloidal solution composed by two populations of NPs, one of 20 nm and the other of 100 nm. From calculated spectra it is possible to see how the presence of large particles substantially alters the shape (FWHM), symmetry and the position of the resultant LSPR peak for the Au NPs, while this effect is screened in the case of Ag NPs due to the large differences in the relative contributions of the two populations. On the other hand, the spectra of the Ag NPs show larger differences in the LSPR intensity. Consequently, one can state that both types of NPs respond optically differently, in terms of the evolution of the UV-vis spectra, in processes involving a mixture of particles of different sizes (but preserving the total mass concentration), including for instance, time-dependent aggregation, Ostwald ripening or sintering.

3.3 Calculated absorbance spectra of monodisperse colloidal solutions of metal NPs considering constant particle number concentration

Figure 3 plots the calculated extinction spectra of Ag and Au NPs for different sizes keeping constant the total number of NPs. Interestingly, in this case, the maximum absorbance value constantly increases as NP size increases, which can be explained by the higher amount of metal atoms present in the solutions with larger NPs. These results are more representative of the growth mechanism of NPs by monomer addition used in many synthetic strategies [45–47]. Thus, when the growth process takes place via the incorporation of monomer from the solution

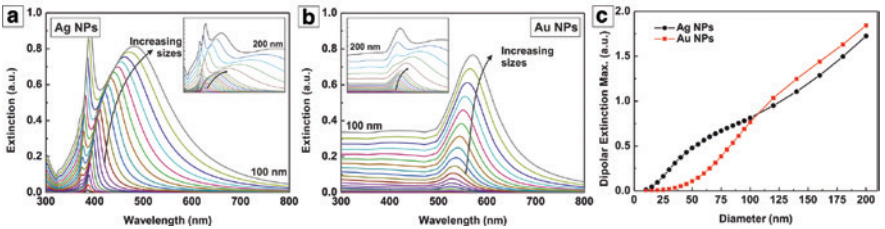

Fig. 3: Calculated extinction spectra of different colloidal solutions of Ag (a) and Au (b) NPs considering a constant particle number concentration. The concentration is $3{\cdot}10^9$ NPs/mL and the light pathway is 1 cm. Dipolar extinction maximum as a function of NP diameter for Ag and Au NPs (c). For small sizes, the maximum increases faster for increasing Ag than Au sizes while for larger sizes both curves evolve similarly which indicates that scattering becomes relevant and dominates the overall shape of the curve.

(the total number of NPs in solution remains unaltered), a constant increasing of maximum extinction should be observed by UV-vis characterization (Figure 3). However, if the growth process is mediated by aggregative or coalescence means, this increase is reversed by the constant decrease of the total number of particles in solution (Figure 1). Another interesting point of Figure 3 is that, by inverting the directions of the arrow in the graphs, the evolution of the spectra is indicative of the possible way that the NPs can follow when dissolving. In this case, the decrease in the extinction intensity should be accompanied by a blue shift in the LSPR position.

3.4 The effect of sample polydispersity

Almost all the physicochemical transformations that NPs can undergo under relevant conditions influence their degree of polydispersity. Thus, it is important to first understand how sample polydispersity may affect the absorbance spectra of different colloidal dispersions of NPs. Since polydispersity is usually obtained from transmission electron microscopy (TEM) analysis, it is here expressed as a standard deviation (SD) of the mean particle diameter.

Figure 4 shows the calculated absorbance spectra of Ag and Au NPs with increasing degree of polydispersity. As can be observed, an increase degree of polidispersity is correlated with a shift of the LSPR peak position together with a damping and loss of the band symmetry, which is translated into wider FWHM. Importantly, as we recently showed [34], the extent in the LSPR shift depends on (i) NP size, (ii) composition and (iii) the optical mode being observed (dipolar vs. quadrupolar). Thus, for small particles, a red-shift on the dipolar LSPR band is observed as increasing polydispersity while it turns to a blue-shift in the case of large particle sizes (Figure 5).

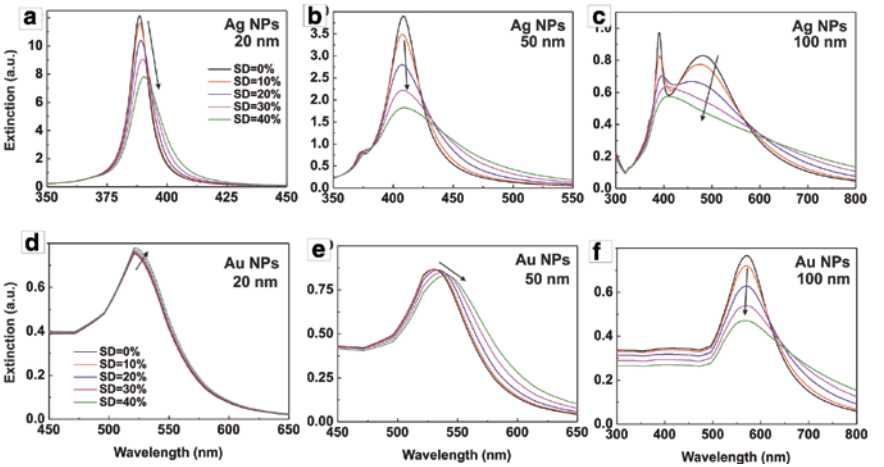

Fig. 4: Calculated extinction spectra of colloidal solutions of Ag and Au NPs with sizes of 20 nm (a, d), 50 nm (b, e) and 100 nm (c, f) and increasing degree of polydispersity (expressed as a standard deviation from NP mean diameter). The concentration of metal atoms is 0.16 mM and the light pathway 1 cm.

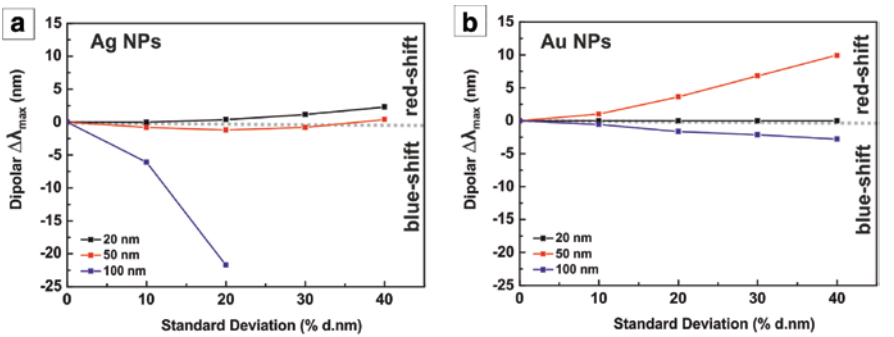

Fig. 5: Evolution of the shift in the LSPR peak position as increasing sample degree of polydispersity for Ag (a) and Au (b) NPs. Polydispersity is expressed as a standard deviation from NP mean diameter. For small particles a red-shift of the dipolar band is observed while it blue-shifts for large particles. Among the polydispersity, the extent of the shifts depends on NP size and composition.

In agreement with that previously discussed in Figure 2, an increase in the polydispersity results in a significant shift in the LSPR peak position in the case of Au, while it is additionally translated into a large decrease in the LSPR intensity in the case of Ag NPs. Finally, and despite the fact that the above calculated optical behaviors are far from ideal (i.e. for many processes the evolution of the

particle sizes cannot be described in terms of a normal distribution), they offer a general overview, especially if considering that all samples are polydisperse to some extent.

3.5 Models for nanoparticle aggregation

The process of aggregation of NPs in colloidal dispersions is complex, due to, in part, the high number of variables that come into play (i.e. particle concentration, surfactant type, electrolytes in solution, chaotic kinetics of aggregation, etc). All of this without taking into account that the process rarely occurs alone and it is usually accompanied by dissolution, oxidation and surface conjugation, among other. Herein we address aggregation in a very simple approximation, considering the resultant clusters as single spherical NPs of equivalent diameter. Such approximation is far from a realistic scenario, and implies that particles completely coalesce to form larger spherical ones, while ignoring any cooperative effect between them or shape transformation. Despite its simplicity, this very basic model allows us to qualitatively describe this process enough to identify some interesting features in the UV-vis spectra evolution and compare it with other experimental observations from the literature. Of course, this model is not applicable to the formation of aggregates with low fractal dimensions, such as chain-like structures, in which additional coupling between optical resonance modes is observed [48]. These limitations are further discussed in detail.

Based on the above considered simplifications, evolution of the UV-vis spectra during NPs aggregation can be approximated to that of NPs with increasing diameters calculated in Figure 1. However, it is known that not all the NPs may evolve uniformly and that during the process of aggregation the polydispersity of the sample increases resulting in a wide range of different sizes. In this regard, for the optical modeling, the fraction of particles in the "aggregated" state were divided in four different populations: (i) single particles and clusters of NPs aggregates composed approximately of (ii) 10, (iii) 100 and (iv) 1000 NPs. Each cluster was considered as a compact sphere with the corresponding equivalent diameter. Varying percentages of the four populations were used to represent different degrees of aggregation and to model the aggregation evolution kinetics of 20 nm and 50 nm NPs.

Two different aggregation kinetics characterized by different time-dependent populations were studied (Figure 6a, b). In the first case, small clusters aggregate faster than large ones, while in the second case the large clusters aggregate faster than the small ones, resulting in two scenarios that aim to exemplify different ways in the kinetic evolution of the aggregation process. From the calculated

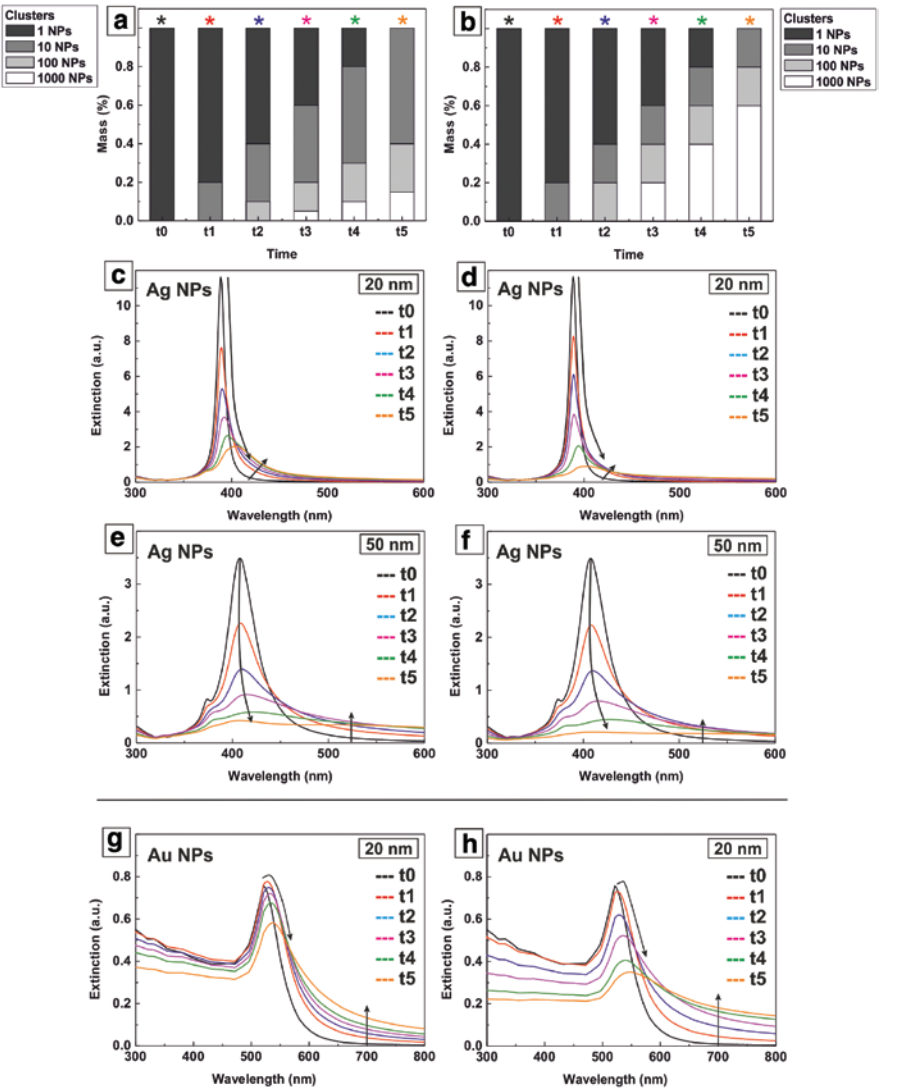

Fig. 6: Evolution of the population of NPs for two different aggregations kinetic profiles (a, b). The clusters are taken as single spheres for modeling calculations. Calculated optical aggregation response of 20 nm Ag NPs (c, d), 50 nm Ag NPs (e, f), and 20 nm Au NPs (g, h). The concentration of Ag atoms during the entire process remains constant at 0.16 mM and the light pathway is 1 cm. Some indicative evidences of aggregation for Ag NPs are: (i) a sharp decrease in the absorbance intensity at the initial states, following by (ii) an increase in the FWHM and the red-shift of the LSPR and (iii) the appearance of a secondary peak (shoulder-like) towards higher wavelength as the extend of the aggregation increases.

spectra shown in Figure 6, it can be seen that the overall optical Ag aggregation profile is mainly dominated by the fraction of individual NPs, and that the differences between both regimes of aggregation are difficult to differentiate. Thus, little differences were found for samples containing small (Figure 6c) and large aggregated clusters (Figure 6d), similarly to the results shown in Figure 2a. High order resonance modes, typically associated with NP aggregates, may be hidden under the predominance of the dipolar peak corresponding to individual small NPs, and the attenuation of this peak as the fraction of single particle decreases due to the presence of aggregates can be considered as the main signature of the aggregation process, in particular at the initial stages. Similar behavior has been seen experimentally in other works for citrate stabilized Ag NPs [48, 49]. From the optical model described above, and the results shown in Figure 6, it is possible to conclude that the aggregation of Ag NPs is not easily detectable by optical means, in particular when comparing with the case of Au NPs (Figure 6g, h). Thus, the well-known optical features of Au aggregation, that is, the red-shift of the LSPR peak, the broadening of the overall spectrum and the increase in the absorbance between 600 and 800 nm are not easily detectable in the case of Ag NPs. This is mainly due to the high extinction efficiency of small Ag NPs that hidden the weak contribution coming from the aggregates. Despite these limitations, some indicative evidences of aggregation of Ag NPs are: (i) a sharp decrease in the particle absorbance intensity at the initial states, followed by (ii) an increase in the FWHM and red-shift of the LSPR and (iii) the appearance of a secondary peak (shoulder-like) towards higher wavelength as the extent of the aggregation increases. Regarding differences between 20 nm and 50 nm, the overall behavior is similar, but modifications in the LSPR peak and FWHM at the initial stages of aggregation are easily detectable in the larger particles since the contribution from the particles and the aggregates are of the same order in this case.

It is worth mentioning here that this optical model is based on spherical compact aggregates, therefore failing to describe branched structures such as those resulting from fast or diffusion limited aggregation regimes. Additionally, the cooperative effect between particles, in terms of an optical response, may in some particular cases, become an important contribution in the extinction spectra, herein omitted, which is usually translated into an additional intense peak at higher wavelengths [50]. The intensity of these peaks is determined by the intensity of NP interaction and usually depends on experimental conditions [48, 50]. Under these circumstances, calculations based on Mie theory should be replaced by a more precise theoretical approximation such as the finite-difference time domain (FDTD) [51]. Finally, it is worth mentioning that numerous works aiming to evaluate the stability of Ag NPs by optical means end up with experimental observations not far from what has been described here [48, 49].

3.6 Models for oxidative dissolution of Ag nanoparticles

Many important properties and potential uses of colloidal Ag NPs dispersions are associated with the activity of the ions released from the particles rather than from the particles themselves [52]. In solution, Ag NPs coexist with their ionic species which exhibit different physicochemical properties and subsequent biological activity. In this context, speciation seems to be determinant when studying the reactivity of NPs in a specific medium. Hence, it is worth trying to predict the evolution of UV-vis spectra upon dissolution of the Ag NPs.

Dissolution processes can be modeled on the basis of a decrease in the average NP size while keeping the total number of particles constant, at least during the first stages, similar to that plotted in Figure 3. In this case, a blue shift in the LSPR while decreasing the extinction intensity was the main characteristic of the spectra evolution. However, as widely discussed in the literature, dissolution of NPs is typically preceded by an oxidation process, and therefore both are optically related [12]. The oxidation of NPs leads to a broadening of the LSPR peak [41, 53] which should be taken into consideration, but more importantly, a strong red-shift (Figure 7a, b) [41, 53–56]. Consequently, when an additional oxide layer is added to the particle surface, the predicted blue-shift in the LSPR peak position turns into a red-shift as the NP size decreases. This red-shift is caused by a modification in the dielectric constant on the surface of the NPs. Additionally, an important limitation of the above described dissolution model is that not all particles dissolve at the same rate. On the contrary, small NPs dissolve faster than larger ones. Moreover, inhomogeneity -mass and thermal gradients- may accentuate these differences. Thus, an increase on the polydispersity degree of the NPs over the course of the dissolution process has been observed experimentally, which should be taken into account when designing optical model systems.

Based on these considerations, a dissolution model characterized by different time-dependent populations of NPs having decreasing sizes and increasing degree of polidispersity was studied. Figure 7c shows the evolution of the particle populations for two different NP sizes: 20 nm (Figure 7d) and 50 nm (Figure 7e). Thus, in the case of 20 nm and 50 nm Ag NPs, individual NPs start to dissolve (**t1**, Figure 7a) leading to three different populations with smaller average sizes which evolve into five populations (**t2**, Figure 7a) and finally nine populations (**t5**, Figure 7a). Obtained spectra suggest that dissolution of NPs is optically correlated with (i) a decrease in extinction intensity together with (ii) an increase in the FWHM, while it is difficult to state whether the LSPR shift to the blue (50 nm) or to the red (20 nm).

All in all, comparing results obtained for aggregation (Figure 6) and dissolution (Figure 7) it is possible to conclude that both processes are optically very

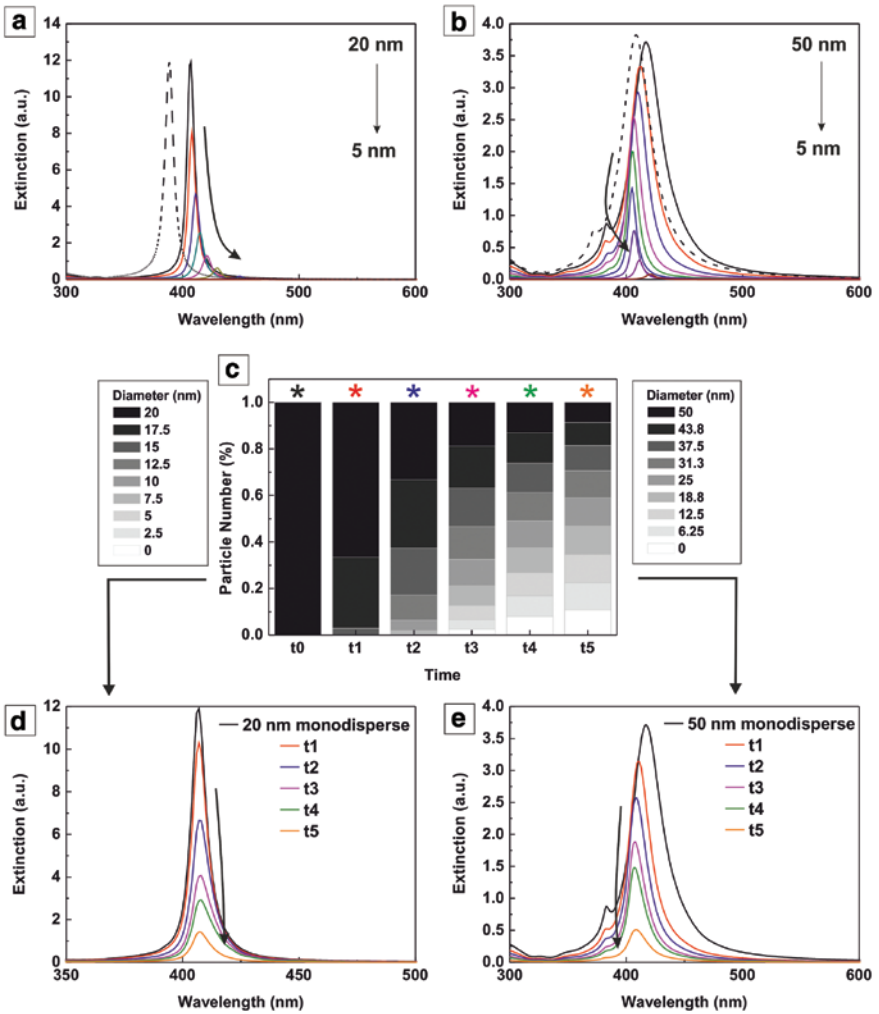

Fig. 7: UV-vis spectra of monodisperse Ag NPs with a 1 nm layer of silver oxide on the surface for decreasing NP size and constant number of particles (a, b). Evolution of the size distribution of Ag NPs in two ideal cases of NP dissolution, 20 nm and 50 nm NPs (c). Evolution of the UV-vis spectra according to the size distribution for particles with an oxide layer. (d, e). The initial mass concentration is 0.16 mM and the light pathway is 1 cm. Dashed lines in (A) refer to the initial state of non-oxidized 20 nm and 50 nm particles.

similar for Ag NPs and share several optical signatures, such as a decrease in the extinction intensity and an increase in the FWHM of the LSPR. So far, the observed red-shift in the former cannot be ascribed exclusively to the aggregation process as oxidative dissolution can also result in the same trend.

Similarly, when particles are coated with an organic layer, such as in the case of protein adsorption, the position of the LSPR band is red-shifted [23, 24]. Thus, proteins present in the media interact with the NPs causing a change in the surrounding refractive index at the particle's surface which is translated into a shift in the LSPR peak. The extent of this shift is fast and depends on the nature of the NP. A recent work reporting how material coating affects the optical properties of the NPs has been recently published [34] and nicely show a higher sensitivity of (i) Ag than Au, (ii) larger than small NPs, (iii) longer than shorter molecules, (iv) SH anchor groups, and (v) low order modes.

Based on previous observations one can conclude that in many situations may be difficult to properly distinguish aggregation and dissolution by optical means (UV-vis spectra) since there is no specific characteristic point that can univocally describe one or the other, or alternatively discard the presence of one of them. Thus, this should be complemented by other analyses, such as TEM analysis or ICP-MS (Inductively-Coupled Mass Spectroscopy) to properly characterize the particle evolution. All in all, the rational analysis and evaluation of the scenario could be used to assess the different possibilities. For instance, if particles are dispersed in cell media, a slow decrease in the intensity of the LSPR peak is indicative of NPs dissolution rather than aggregation, since the rapid coating of Ag NPs by media proteins (so-called protein corona) may prevent NPs from aggregation.

4 Conclusions

Optical properties of noble metal nanoparticles are very sensitive to physicochemical transformation such as aggregation, dissolution, oxidation, and protein adsorption. UV-vis spectroscopy is a powerful tool to characterize the evolution of the particles in a colloidal dispersion after being dispersed in different media. It is rapid, so it can be done *in situ* and does not require a complex preparation of the sample. However, the precise and unequivocal differentiation among these processes is rather complicated and additional techniques, such as TEM analysis or ICP-MS may be necessary to accompany the UV-vis results in order to properly characterize the particle evolution.

So far, the most indicative evidences in the UV-vis spectra of Ag NP aggregation are: (i) a decrease in the extinction intensity, (ii) a red-shift in the LSPR peak position, (iii) an increase in the FWHM and (iv) the appearance of an additional shoulder or absorbance peak at long wavelength. The first three optical signatures are shared with the oxidative dissolution of the particles, therefore making

difficult to differentiate both processes only by UV-vis analysis. Additionally, due to the higher Q_{ext} of small Ag particles compared to the large ones, a small fraction of these does not have an important contribution to the absorbance spectra making difficult to optically identify their presence in the final sample. This problem is less critical in the case of Au NPs since they have a Q_{ext} of comparable magnitude for a wider range of sizes.

On the other hand aggregation processes rarely occur alone. On the contrary, oxidation and subsequent dissolution of the particles typically take place at the same time and can even contribute to it [57, 58]. An example is the aggregation of Ag NPs dispersed in water at atmospheric conditions after exposure to chlorine-rich salts. In these experiments, the compression of the stabilizing electrical double layer due to the presence of ions promotes aggregation of NPs. In parallel, the oxygen dissolved in the medium oxidizes silver NP surface and further reacts with chlorine ions to form insoluble species, such as AgCl [59]. As a result, the aggregation, oxidation and dissolution of Ag NPs take place simultaneously. The temporal overlapping of all of these processes, not only in complex media but also in very simple scenarios, makes the optical properties of Ag NPs, in particular the UV-vis spectra and the LSPRs difficult to predict. Moreover, the presence of scattering signals at higher wavelengths cannot be univocally associated with the aggregation of Ag NPs since this scattering may also come from the insoluble silver salts present in the media.

Acknowledgments: We acknowledge financial support from the Spanish Ministerio de Ciencia e Innovación (MICINN) (MAT2012-33330) (MAT2015-70725-R) and from the Catalan Agència de Gestió d'Ajuts Universitaris i de Recerca (AGAUR) (2014-SGR-612). Financial support from the FutureNanoNeeds (FP7-NMP-2013-LARGE-7) Project financed by the European Community under the FP7 Capacities Programme is gratefully acknowledged. N.G.B. acknowledges financial support by MINECO through the Ramon y Cajal program (RYC-2012- 10991) and by the European Commission Seventh Framework Programme (FP7) through the Marie Curie Career Integration Grant (322153-MINE).

References

1. K. Chaloupka, Y. Malam, A. M. Seifalian, Trends Biotechnol. **28** (2010) 580.
2. X. Chen, H. J. Schluesener, Toxicol. Lett. **176** (2008) 1.
3. G. A. Sotiriou, S. E. Pratsinis, Curr. Opin. Chem. Eng. **1** (2011) 3.
4. B. Reidy, A. Haase, A. Luch, K. Dawson, I. Lynch, Materials **6** (2013), 2295.
5. N. Hadrup, H. R. Lam, Regul. Toxicol. Pharmacol. **68** (2014) 1.

6. F. Gottschalk, B. Nowack, J. Environ. Monit. **13** (2011) 1145.
7. Y. Teow, P. V. Asharani, M. P. Hande, S. Valiyaveettil, Chem. Commun. **47** (2011) 7025.
8. I. A. Mudunkotuwa, V. H. Grassian, J. Environ. Monit. **13** (2011) 1135.
9. B. Nowack, H. F. Krug, M. Height, Environ. Sci. Technol. **45** (2011) 1177.
10. N. G. Bastús, E. Casals, I. Ojea, M. Varon, V. Puntes, The Reactivity of Colloidal Inorganic Nanoparticles, In *The Delivery of Nanoparticles*, A. A. Hashim, Ed. InTech, Rijeka, Croatia (2012).
11. E. Casals, E. Gonzalez, V. F. Puntes, J. Phys. D. Appl. Phys. **45** (2012) 443001.
12. J. Liu, R. H. Hurt, Environ. Sci. Technol. **44** (2010) 2169.
13. L. V. Stebounova, E. Guio, V. H. Grassian, J. Nanopart. Res. **13** (2011) 233.
14. X. Wang, Z. Ji, C. H. Chang, H. Zhang, M. Wang, Y.-P. Liao, S. Lin, H. Meng, R. Li, B. Sun, L. V. Winkle, K. E. Pinkerton, J. I. Zink, T. Xia, A. E. Nel, Small **10** (2014) 385.
15. A. D. Maynard, D. B. Warheit, M. A. Philbert, Toxicol. Sci. **120** (2011) S109.
16. Z.-m. Xiu, Q.-b. Zhang, H. L. Puppala, V. L. Colvin, P. J. J. Alvarez, Nano Lett. **12** (2012) 4271.
17. J. L. Axson, D. I. Stark, A. L. Bondy, S. S. Capracotta, A. D. Maynard, M. A. Philbert, I. L. Bergin, A. P. Ault, J. Phys. Chem. C **119** (2015) 20632.
18. S. Elzey, V. H. Grassian, J. Nanopart. Res. **12** (2010) 1945.
19. K. Loza, J. Diendorf, C. Sengstock, L. Ruiz-Gonzalez, J. M. Gonzalez-Calbet, M. Vallet-Regi, M. Koller, M. Epple, J. Mater. Chem. B **2** (2014) 1634.
20. B. Simoncic, B. Tomsic, Text. Res. J. **80** (2010) 1721.
21. J. W. Alexander, Surg. Infect. **10** (2009) 289.
22. S. Chernousova, M. Epple, Angew. Chem. Int. Ed. **52** (2013) 1636.
23. E. Casals, T. Pfaller, A. Duschl, G. J. Oostingh, V. Puntes, ACS Nano **4** (2010) 3623.
24. E. Casals, T. Pfaller, A. Duschl, G. J. Oostingh, V. F. Puntes, Small **7** (2011) 3479.
25. F. Ding, S. Radic, R. Chen, P. Chen, N. K. Geitner, J. M. Brown, P. C. Ke, Nanoscale **5** (2013) 9162.
26. R. Podila, R. Chen, P. C. Ke, J. M. Brown, A. M. Rao, Appl. Phys. Lett. **101** (2012) 263701.
27. E. Casals, V. F. Puntes, Nanomedicine (Lond) **7** (2012) 1917.
28. I. Lynch, T. Cedervall, M. Lundqvist, C. Cabaleiro-Lago, S. Linse, K. A. Dawson, Adv. Colloid Interface Sci. **134–135** (2007) 167.
29. S. K. Mwilu, A. M. El Badawy, K. Bradham, C. Nelson, D. Thomas, K. G. Scheckel, T. Tolaymat, L. Ma, K. R. Rogers, Sci. Total Environ. **447** (2013) 90.
30. C. Burda, X. Chen, R. Narayanan, M. A. El-Sayed, Chem. Rev. **105** (2005) 1025.
31. X. Huang, S. Neretina, M. A. El-Sayed, Adv. Mater. **21** (2009) 4880.
32. X. Lu, M. Rycenga, S. E. Skrabalak, B. Wiley, Y. Xia, Annu. Rev. Phys. Chem. **60** (2009) 167.
33. N. J. Halas, S. Lal, W.-S. Chang, S. Link, P. Nordlander, Chem. Rev. **111** (2011) 3913.
34. N. G. Bastus, J. Piella, V. Puntes, Langmuir **32** (2016) 290.
35. B. J. Wiley, S. H. Im, Z.-Y. Li, J. McLellan, A. Siekkinen, Y. Xia, J. Phys. Chem. B **110** (2006) 15666.
36. J. P. Camden, J. A. Dieringer, J. Zhao, R. P. Van Duyne, Acc. Chem. Res. **41** (2008) 1653.
37. S. Lal, S. E. Clare, N. J. Halas, Acc. Chem. Res. **41** (2008) 1842.
38. R. A. Petros, J. M. DeSimone, Nat. Rev. Drug Discov. **9** (2010) 615.
39. B. Tejerina, T. Takeshita, L. Ausman, G. C. Schatz, Nanosphere Optics Lab. Field Simulator. 2008.
40. B. K. Juluri, J. Huang, L. Jensen, Extinction, Scattering and Absorption efficiencies of single and multilayer nanoparticles. 2016.
41. Y. D. Yin, Z. Y. Li, Z. Y. Zhong, B. Gates, Y. N. Xia, S. Venkateswaran, J. Mater. Chem. **12** (2002) 522.

42. U. Kreibig, L. Genzel, Surf. Sci. **156** (1985) 678.
43. C. Noguez, J. Phys. Chem. C **111** (2007) 3806.
44. W. Haiss, N. T. K. Thanh, J. Aveyard, D. G. Fernig, Anal. Chem. **79** (2007) 4215.
45. N. G. Bastús, J. Comenge, V. F. Puntes, Langmuir **27** (2011) 11098.
46. N. G. Bastús, F. Merkoçi, J. Piella, V. Puntes, Chem. Mater. **26** (2014) 2836.
47. J. Piella, N. G. Bastus, V. Puntes, Chem. Mater. **28** (2016) 1066.
48. R. Gill, L. Tian, W. R. C. Somerville, E. C. Le Ru, H. van Amerongen, V. Subramaniam, J. Phys. Chem. C **116** (2012) 16687.
49. S. Botasini, E. Méndez, J. Nanopart. Res. **15** (2013) 1.
50. M. M. Jiang, H. Y. Chen, B. H. Li, K. W. Liu, C. X. Shan, D. Z. Shen, J. Mater. Chem. C **2** (2014) 56.
51. V. Chegel, O. Rachkov, A. Lopatynskyi, S. Ishihara, I. Yanchuk, Y. Nemoto, J. P. Hill, K. Ariga, J. Phys. Chem. C **116** (2012) 2683.
52. S. Kittler, C. Greulich, J. Diendorf, M. Koeller, M. Epple, Chem. Mater. **22** (2010) 4548.
53. M. Chen, L.-Y. Wang, J.-T. Han, J.-Y. Zhang, Z.-Y. Li, D.-J. Qian, J. Phys. Chem. B **110** (2006) 11224.
54. A. Henglein, Chem. Mater. **10** (1998) 444.
55. S. Kapoor, Langmuir **14** (1998) 1021.
56. A. Kuzma, M. Weis, S. Flickyngerova, J. Jakabovic, A. Satka, E. Dobrocka, J. Chlpik, J. Cirak, M. Donoval, P. Telek, F. Uherek, D. Donoval, J. Appl. Phys. **112** (2012).
57. X. Li, J. J. Lenhart, H. W. Walker, Langmuir **28** (2012) 1095.
58. X. Li, J. J. Lenhart, H. W. Walker, Langmuir **26** (2010) 16690.
59. J. Y. Liu, D. A. Sonshine, S. Shervani, R. H. Hurt, ACS Nano **4** (2010) 6903.